Research Article

Advances in Mechanical Engineering

Advances in Mechanical Engineering
2024, Vol. 16(9) 1–15

DOI: 10.1177/16878132241281079
journals.sagepub.com/home/ade
Sage

Self-lock carrier: Realize low-backlash characteristic in 3 K planetary gearbox

Zilong Ling[1], Dong Xiao[2], Lei Zhao[1], Yue Li[1], Zhongzan Ji[1], Siyuan Xi[1], Xiaofeng Xia[1] and Yi Zhou[1,3]

Abstract

Advanced manufacturing equipment heavily relies on gearboxes for optimal performance, especially in heavy-duty applications like industrial robot joints and advanced machine tools where precision and stiffness are paramount. While harmonic and cycloid gearboxes are common for their low backlash characteristic, conventional 3 K planetary gears excel in efficiency, torque density and stiffness but they are rarely utilized in high precision scenario due to backlash issue. In this study, a deformable planet carrier system (DPCS) is proposed for backlash restrain by center distance compensation. The DPCS incorporates a self-lock design, preserving low backlash feature while upholding load capacity and stiffness, meeting the demands of precision industrial equipment. To illustrate its principles, statics models demonstrate its force analysis, and FEM simulations reveal its self-lock feature. Backlash compensation model theoretically analyzes its anti-backlash effect from kinematics and geometry aspects. To validate its feasibility, the first prototype is manufactured and designated as H3K-40K-104. Experiment result prove that prototype achieves significant low backlash characteristic, with the maximum dynamic transmission error (DTE) of 20.5 arcsec and backlash of 6.561 arcsec. Stiffness hysteresis curve indicates a minimal lost motion of 20.01 arcsec. This paper provides an effective method to greatly refine precision performance in 3 K gear trains.

Keywords

3 K planetary gear, deformable carrier, self-lock, robotic, anti-backlash, H3K Gear

Date received: 15 April 2024; accepted: 16 August 2024

Handling Editor: Aarthy Esakkiappan

Introduction

Precision reduction gears serve as the cornerstone of advanced equipment, playing a pivotal role in a diverse range of applications, notably in industrial robots, machine tools, and vehicles.[1] Meticulously manufactured gears are essential for ensuring high precision and efficiency, and being indispensable components in modern machinery. Industrial robots, for instance, are highly relied on precision reduction gears for accurate and seamless movement.[2] These gears empower the robots to execute intricate tasks with exceptional precision, spanning from assembling delicate components to performing precise surgical procedures.[3] Industrial robots require diverse gearbox based on the torque and stiffness requirements of their joints, yet space constraints necessitate more compact and integrated designs.[1] High torque density enables the robots to

[1]Department of R&D, AICI Technology (Ningbo) Co., Ltd., Shenzhen, China
[2]Gearbox Development and Application Team of KUKA China R&D, KUKA Robotics Guangdong Co., Ltd., Foshan, China
[3]Department of Mechanical Engineering, The Hong Kong Polytechnic University, Hong Kong, China

Corresponding author:
Yi Zhou, AICI Technology (Ningbo) Co., Ltd., Building B, Kutuo Intelligent Manufacturing Industrial Park, No.26, Xinhe Avenue, Baoan District, Shenzhen, China.
Email: zhouyi@h-nnn.com

handle substantial loads with compact structure, while broad reduction ratio range facilitates for a wide spectrum of speeds, enhancing the robot's versatility and adaptability.[4–6] Within the domain of machine tools, these performances play an equal vital role. Accurate power transmission ensures that the machine tools operate at the desired speed and torque, which is particularly critical in applications like milling, drilling, and grinding, where precision and consistency are paramount. Sufficient torque capacity enables the machine tools to tackle heavy-duty operations, while their expansive reduction ratio range offers the flexibility to adjust the speed and torque as per the requirements of the task at hand.[7]

Generally, gearbox selection for robot prioritizes torque density, ratio range and torsional stiffness, which are pivotal factors influencing robot R&D. Cycloid gearboxes have complicated inner structure and various components, which makes it heavy and increases its manufacturing and maintenance cost.[8] Harmonic gearboxes have low torsional stiffness and load capacity, which limits its industrial applications.[9] 3 K planetary gear is a compact mechanism that combines excellent torsional stiffness, load capacity and torque density, which is capable of meeting these requirements of advanced equipment. Current 3 K planetary gear research also employs several approaches to further enhance its performances, and exploit its potential: (i) asymmetric teeth design can boost load capacity[10]; (ii) tooth profile modification can improve transmission efficiency[11]; (iii) improvement in tooth contact and load distribution conditions.[12,13] However, cycloid gearboxes and harmonic gearboxes are extensively utilized in modern robotic systems[9] due to their low backlash characteristic. 3 K planetary gearbox adoption in advanced robots remains limited due to challenges in achieving the necessary precision performance.

Backlash stands out as a critical factor leading to precision degradation within gear trains. From a statics perspective, lost motion serves as an indicator highly tied to backlash during repetitive movement and changes in torque direction. It represents the angular displacement where tooth come through without transmitting any force, ultimately causing accuracy loss and response hysteresis. From a dynamic perspective, backlash leads to tooth impact and vibration phenomena. This is primarily due to the velocity difference at gear mate, deteriorating contact condition and inducing pitting and spall on tooth profile.[14] It causes impact, vibration and noise during frequent bidirectional movement, ultimately impeding transmission accuracy and responsiveness.[15] Over time, gear wear and the error of initial machining and assembling contribute to irreversible increases in backlash, causing torque transmission to become nonlinear and compromising accuracy.

In order to mitigate the influence of backlash in industrial applications, some researchers focus on monitoring and predicting gear wear propagation by vibration analysis techniques, which enables to perform timely maintenance according to useful remaining lifetime estimation.[16] For example, (i) Sreepradha et al. posed artificial neural networks predict film thickness and lubrication to assess wear conditions,[17] (ii) Feng et al. introduced digital twin technologies establish real-time synchronization between physical and virtual models, enabling continuous assessment of surface degradation and gear wear.[18] Accurate lifetime prediction and timely gearbox replacement are effective strategies for maintaining optimal performance in industrial equipment. Intelligent and real-time gear assessment also benefits engineers to judge the wear progression in gear system. However, other researchers tend to focus on proposing mechanical and algorithmic solutions to address backlash issues directly: (i) backlash compensation algorithm in control system from Nordin and Gutman[19]; (ii) traction drive mechanisms proposed by Oba and Fujimoto[20,21]; (iii) flexible anti-backlash mechanisms on strain wave gear reducer invented by Ling et al.[22] Although current studies offer various thinking to realize low backlash characteristic, many structures rely on complicated components, advanced machining techniques and expensive control systems, which make them impractical and unreliable. In relevant research, flexible anti-backlash mechanism normally shows higher precision improvement, but it also compromises torsional stiffness.[23–25] Apparently, a substantial decrease in the overall performance of the gearbox undermines the industrial significance of the anti-backlash mechanism. Low stiffness characteristic enlarges the precision loss under heavy-duty work condition due to it induces larger deformation on gear trains, despite the backlash is well restrained. It impedes the anti-backlash gearbox from widely applied in industrial equipment.

To fill the research gap, this study aims to introduce a deformable planet carrier, which equips a self-lock taper sleeve, forming an innovative deformable anti-backlash system. Deformable planet carrier realizes center distance adjustment to compensate backlash, and self-lock design avoids the carrier shrinkage under load condition. Our prototype adopts Wolfrom -based design (Figure 1), first proposed by Ulrich Wolfrom in Germany in 1912,[26] which is used to validate DPCS's feasibility. In experiment, this prototype, designated as H3K Gear, reveals outstanding precision performance, and represents a clear low-backlash characteristic without compromising torsional stiffness and load capacity. The lost motion and dynamic transmission error can be maintained within 25 arcsec.

In section 2, a basic H3K Gear framework is given. Section 3 introduces the principle of DPCS, its statics models and backlash compensation model. The effect

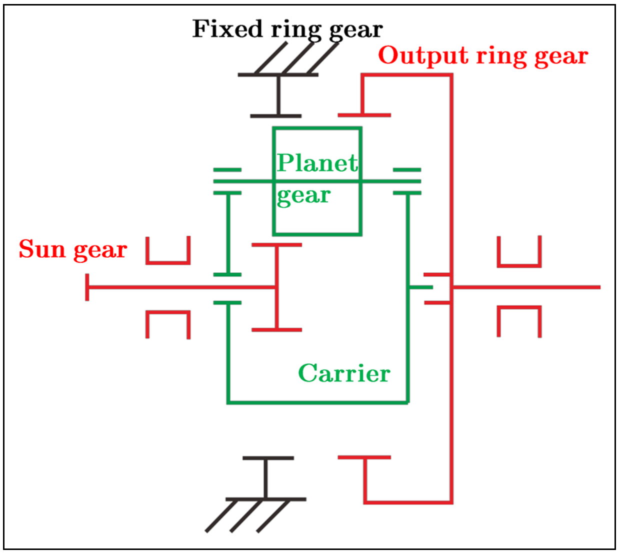

Figure 1. Wolfrom-based 3 K planetary gear design.

of self-lock taper sleeve and center distance change then is revealed by Finite Element Method (FEM). In section 4 & section 5, prototype experiments are conducted to further prove the feasibility of DPCS. In the end, section 6 provides a detailed discussion and conclusion about this study.

Basic H3K Gear structure framework

Figure 1 illustrates the layout comprising two stages: a primary planetary gear train and an additional planet- & output-ring gear stage. Within the transmission trains, sun- and output-ring gear function as the input and output shaft respectively. The planet gears situated at the deformable planet carrier, engage with both the fixed-ring gear and output-ring gear simultaneously, while orbiting around the sun gear. The tooth profile adopts an involute shape with a helical angle, enhancing the contact ratio and ensuring seamless transmission. Equations (1)–(3) give a typical reduction ratio relationship in 3 K planetary gearbox. In this study, our anti-backlash mechanism is equipped at the second stage. Variables required in derivation process are defined in Table 1.

$$\begin{cases} \dfrac{\omega_s - \omega_c}{\omega_p - \omega_c} = -\dfrac{z_p}{z_s} \\ \dfrac{\omega_p - \omega_c}{\omega_o - \omega_c} = \dfrac{z_o}{z_p} \\ \dfrac{\omega_p - \omega_c}{\omega_f - \omega_c} = \dfrac{z_f}{z_p} \\ \omega_f = 0 \end{cases} \tag{1}$$

H3K Gear can be transferred to a fixed-axis gear train, and its transmission ratio is defined by equation (1), where the rotational speed of fix ring gear ω_f is zero. Subsequently, equation (2) can be derived accordingly.

Table 1. Variable naming list.

Component	Rotational speed	Number of teeth (NOT)
Sun gear	ω_s	z_s
Planet gear	ω_p	z_p
Carrier	ω_c	-
Fix ring gear	ω_f	z_f
Output ring gear	ω_o	z_o

$$\begin{cases} \dfrac{\omega_c}{\omega_s} = \dfrac{z_s}{z_s + z_f} \\ \dfrac{\omega_o}{\omega_s} = \dfrac{z_s \cdot (z_o - z_f)}{z_o \cdot (z_s + z_f)} \\ \dfrac{\omega_p}{\omega_s} = \dfrac{z_s \cdot (z_p - z_f)}{z_p \cdot (z_s + z_f)} \\ \dfrac{\omega_p - \omega_c}{\omega_s} = -\dfrac{z_s \cdot z_f}{z_p \cdot (z_s + z_f)} \end{cases} \tag{2}$$

For each reduction stage, total ratio i can be divided as a product of two ratio components i_1 and i_2:

$$\begin{cases} i_1 = \dfrac{z_f}{z_s} + 1 \\ i_2 = \dfrac{z_o}{z_o - z_f} \\ i = i_1 i_2 \\ \dfrac{z_o - z_f}{N_p} = C \end{cases} \tag{3}$$

where C is an integer, N_p is the amount of planet gear.

Anti-backlash design

DPCS principles

The Deformable Planet Carrier System (DPCS) is the key component within the H3K Gear, facilitating the pursuit of higher transmission precision and reduced lost motion. Figure 2(a)) illustrates the innovative system comprises a self-lock taper sleeve, planet gears, spring washer, and a deformable carrier, effectively replacing the conventional rigid carrier to restrain backlash. As shown in Figure 2(b)), deformable carrier utilizes springs to connect planet gears, facilitating the adjustment of their radial positions by varying the pitch circle circumference of the three planet shafts. Backlash existing between planet- and ring gears is refilled in this process.

Maintain the anti-backlash state under heavy load is the kernel of this mechanism. Generally, designed spring stiffness is unable to prevent carrier shrinkage under heavy torque, compensated backlash then reappears along with the spring shrinkage under load. To address this issue, taper sleeve is designed with sufficient stiffness to support carrier. Spring washers

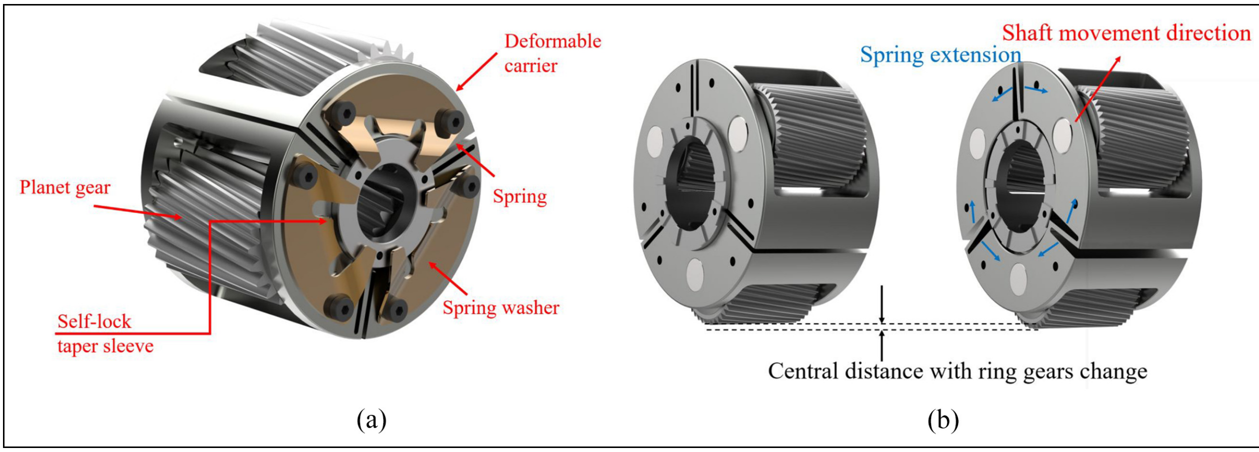

Figure 2. The conceptual diagram of (a) DPCS structure; (b) its anti-backlash process.

are uniformly positioned along the carrier's bottom using screws to push the taper sleeve inward through preload. In the presence of friction at the contact surface, cone angle generates a self-lock effect that prevents the taper sleeve from disengaging under load. Despite the spring stiffness is weak, the taper sleeve effectively impedes large carrier shrinkage. It thereby prevents the resurgence of refilled center distance and compensated backlash. The H3K planetary gearbox is equipped with DPCS, thus endowing it with anti-backlash properties.

In the backlash refilling process, the planet gears must experience parallel displacement along the radial direction without exhibiting tilt behavior. To achieve this target, stringent constraints are placed on machining errors occurring on the contact surface between taper sleeve and deformable carrier. A matching procedure is wielded between taper sleeve and deformable carrier based on measured machining error. This step is crucial to prevent uneven deformation of carrier after taper sleeve insertion, which could lead to planet tilting and the irregular engagement, resulting in increased contact stress, vibration and potential gear failure. Additionally, by implementing tooth profile modifications and axial adjustments, the contact conditions between the planet gear and internal ring gears can be improved. Compared with the traditional rigid carrier design, this deformable carrier design maintains the same level of support effect for the planet gear without induce extra distortion, tilting and shifting, preserving tooth load capacity. In terms of spring types, the conceptual diagram employs a straightforward Z-shaped design to illustrate its operational principle.

DPCS statics model

Figure 3 illustrates the force analysis diagrams of DPCS at steady state. Planet gears are evenly distributed along the carrier and separated by springs. Assume the engagement point locates at pitch circle, the friction coefficient on tooth surface as μ, then equilibrium equations are derived according to Figure 3(a)). The equation (4) establishes the relationship between input torque and output torque in H3K Gear, equation (5) and (6) treat planet shaft as research object, and analyze the force along radial and tangent direction respectively. DPCS does not participate in torque transmission process, as spring forces acts as an inner force.

$$
\begin{cases}
F_f\left(1 + j\mu\tan\alpha_{fp}\right) - F_o\left(1 + k\mu\tan\alpha_{op}\right) \\
\quad - F_s\left(1 + l\mu\tan\alpha_{sp}\right) = 0 & (4) \\
i\left[-F_f\left(\cos\alpha_{fp} + j\mu\sin\alpha_{fp}\right) + F_o\left(\cos\alpha_{op} + k\mu\sin\alpha_{op}\right)\right] \\
\quad - F_s\left(\cos\alpha_{sp} + l\mu\sin\alpha_{sp}\right) = F_t & (5) \\
\quad -F_f\left(\sin\alpha_{fp} - j\mu\cos\alpha_{fp}\right) - F_o\left(sin\alpha_{op} - k\mu\cos\alpha_{op}\right) \\
\quad + F_s\left(sin\alpha_{sp} - l\mu\cos\alpha_{sp}\right) = F_r & (6)
\end{cases}
$$

Where $j, k, l = 1, -1$ according to if the friction torque direction is as same as that of meshing force. $i = 1$ if the input shaft rotates on the same direction with output shaft, otherwise $i = -1$. Dash line represents possible friction force directions. F_f, F_o, F_s represent the normal pressure of fix ring gear, output ring gear and sun gear to planet gear respectively. F_r and F_t are the resultant reaction force of planet shaft to planet gear along radial and tangential direction respectively.

Self-lock taper sleeve maintains carrier position after backlash compensation, as Figure 3(b)). When finish installation, spring washer imposes F_a to taper sleeve at its bottom, even reaction pressure p is perpendicular with the contact surface, which derives two components p_r and p_a along axial and radial direction. Assume the friction coefficient is μ_c, and its equivalent friction angle is θ_c. Force balance equations then can be established as equation (7-9). Generally, designed cone angle α should be much bigger than calculated value as lubrication condition may change due to

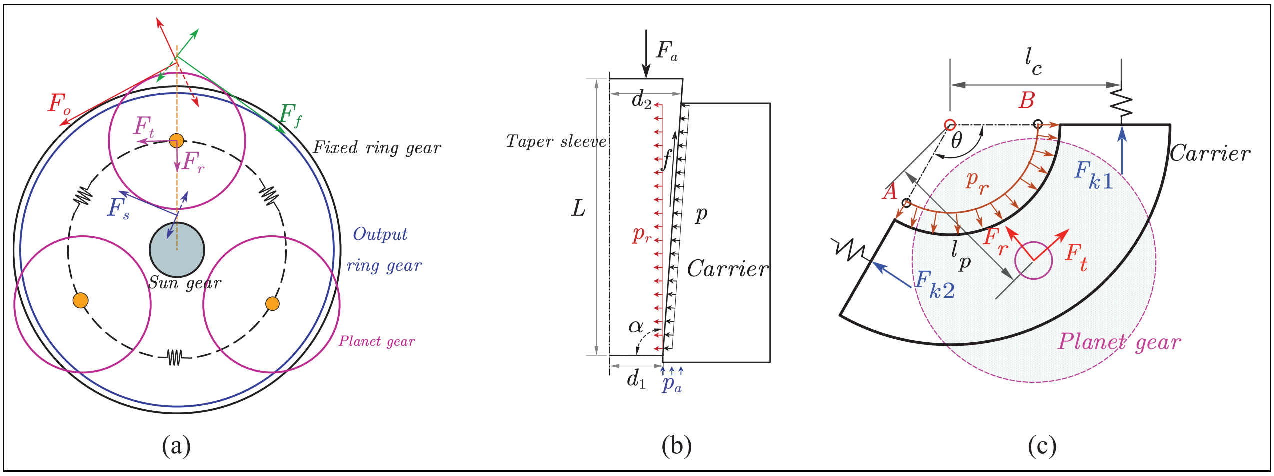

Figure 3. Force analysis diagrams: (a) entire force analysis under load; (b) taper sleeve self-lock force analysis; (c) one-third carrier force analysis.

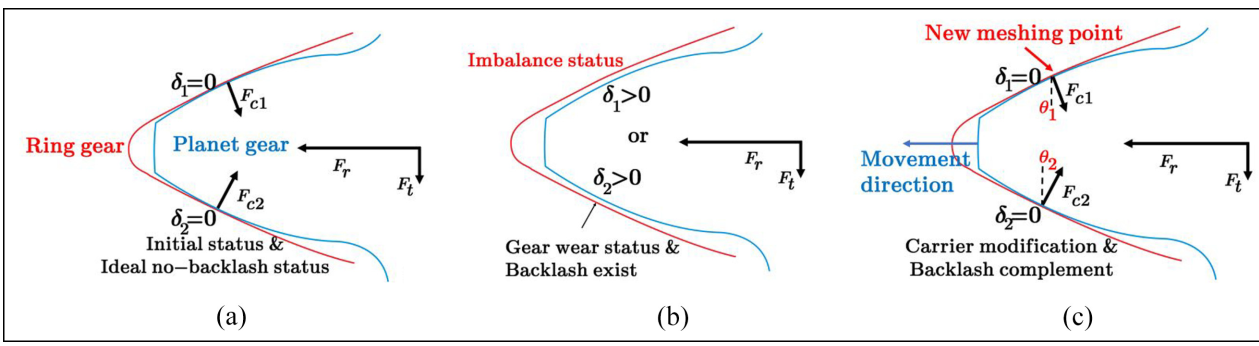

Figure 4. Ideal process of tooth movement and backlash complement: (a) Initial non-backlash status under bilateral meshing, (b) Tooth profile degradation generates backlash when working, and (c) Carrier modification adaptively compensates the backlash and forms new bilateral meshing status.

working temperature, lubricant property and machining roughness.

$$\begin{cases} p = \dfrac{2F_a \cos\theta_c \cos\alpha}{\pi(d_1 + d_2)L\sin(\theta_c + \alpha)} & (7) \\ \theta_c = \arctan\mu_c & (8) \\ p_r = p\sin\alpha & (9) \end{cases}$$

From the theoretical basis above, DPCS has two different mechanic models in anti-backlash process and loading process, respectively.

Anti-backlash process. Anti-backlash process is carried out under no-load condition, self-lock taper sleeve squeezes carrier and extends its springs after installation. The force equilibrium equations (10) and (11) of one-third carrier can be derived from Figure 3(c)). Note that $F_{ki} = K_i x_i (i = 1, 2, 3)$ represents spring tension force of each carrier spring, where K_i is spring stiffness. F_r is reaction force derived from tooth engagement.

$$\begin{cases} F_{k1}l_c - F_{k2}l_c = F_t l_p & (10) \\ \oint \boldsymbol{p}_r ds - (F_{k1} + F_{k2})\cos\dfrac{\theta}{2} = F_r & (11) \end{cases}$$

Consider $F_t = 0$, compensated center distance has relationship, notes as equation (12).

$$\Delta j = \frac{\sum x_i}{2\pi} \quad (12)$$

$$\begin{cases} F_{c1}\sin\theta_1 + F_{c2}\sin\ \theta_2 = F_r \\ \delta_i = 0(i = 1, 2) \\ F_{c1}\cos\theta_1 - F_{c2}\cos\ \theta_2 = F_t \end{cases} \quad (13)$$

Figure 4 describes the process of backlash generation and compensation. Circumferential backlash on each side of tooth profile is symbolized as δ_1 and δ_2, while the engagement forces on both sides of profile are noted as F_{c1} and F_{c2}, respectively. Force equilibrium equation (13) is established. Involute property enables force direction always along its meshing line, so engagement phase has no influence on this force analysis.

Consider equation (7), the critical anti-backlash point is found when $F_r = 0$, and the maximum Δj is critical compensated center distance. Within this critical point, DPCS exhibits significant anti-backlash characteristic, and imposes little contact force at tooth surface.

Loading process. DPCS reveals its self-lock characteristic under loading condition. On the contact surface between taper sleeve and carrier, equation (14) is derived according to Figure 3(b)).

$$p \cos \alpha < p \tan \theta_c \sin \alpha + F_a \tag{14}$$

Therefore, taper sleeve keeps self-lock status to prevent carrier shrinkage under loading condition, radial force F_r at planet shaft, generated by torque transmission process, balances with that of other shafts through self-lock taper sleeve. Meanwhile, spring washer can push taper sleeve inside in the wake of carrier extension. This anti-backlash mechanism plays different roles in two processes, which is backlash compensation and precision retention under load.

FEM result of self-lock taper sleeve

FEM simulations serve to validate the feasibility of DPCS theoretically based on prototype H3K-40K-104, and a FEM model of gear system is established, comprising the DPCS, sun-, fixed ring- and output ring gear. Table 2 gives its detailed design parameters.

Table 2. Major design parameters of H3K-40K-104 prototype.

Characteristic	Symbol	Value
Reduction ratio	i	1:104
Rated torque [*Nm*]	T_r	400
Number of teeth (NOT) Sun gear	z_s	11
NOT Planet gear	z_p	21
NOT Fixed ring gear	z_f	55
NOT Output ring gear	z_o	52
Planet gear number	N_p	3
Transverse modulus	m_t	1.56
Transverse pressure angle	α_t	20.3°
Designed no backlash center distance	a_0	26.1
Weight [*kg*]	-	4.8
Diameter [*mm*]	-	145
Height [*mm*]	-	77

The initial center distance between the planet gears and ring gears is intentionally set slightly smaller than the ideal non-backlash status to account for a certain tooth backlash. The simulation commences from establishing the initial status, defining essential boundary conditions, regulating element interference, and setting contact parameters.

Subsequently, a 1 kN external force is applied to push the taper sleeve inward, which is facilitated by spring washers. In the final step, a rated torque of 400 Nm is applied to the output ring gear, with the input shaft fixed as boundary conditions. Two different friction coefficients are considered: 0.15 and 0.01. These values determines whether the taper sleeve attains self-lock or non-self-lock status, respectively. Then, the post-processing results of displacement along axial and radial direction are listed in Table 3.

Figure 5 illustrates the process of taper sleeve insertion under external force, showcasing a 1.254 mm axial movement of the taper sleeve. In the self-lock status, the taper sleeve maintains its position at 1.2496 mm under load. By comparison, a distinct taper sleeve extrusion behavior occurs in the non-self-lock status when subjected to a load, and the taper sleeve moves 1.0309 mm toward outside. In Figure 6, the evolution of shaft pitch diameters under different statuses is depicted. Taper sleeve insertion extends the carrier spring, and planet shaft move radially with approximate 0.117 mm. The self-lock status exhibits significant radial stiffness, with the shaft effectively maintaining this movement at 0.096 mm under a 400 Nm torque. This shaft displacement effectively preserves the central distance between the planet gear and the two ring gears, showcasing an anti-backlash characteristic. However, the non-self-lock status fails to prevent carrier shrinkage, leading to a 0.118 mm inward movement of the shaft. Figure 7 demonstrates tooth engagement status, both sliding and sticking status represent contact establishment. Before taper sleeve insertion, half of tooth has contacted bilaterally, and the other half of tooth exist backlash. Then, carrier extension increases tooth contact area, and slight preload enables to well restrain backlash.

Backlash compensation model

Backlash typically arises at each gear pair owing to manufacturing and assembly variations, but the

Table 3. The FEM displacement result of DPCS after taper sleeve insertion.

	Free-load status 0 Nm torque	Self-lock status under 400 Nm torque	Non-self-lock status under 400 Nm torque
Axial displacement of taper sleeve (mm)	1.254	1.2496	−1.0309
Radial displacement of planet shaft (mm)	0.117	0.096	−0.118

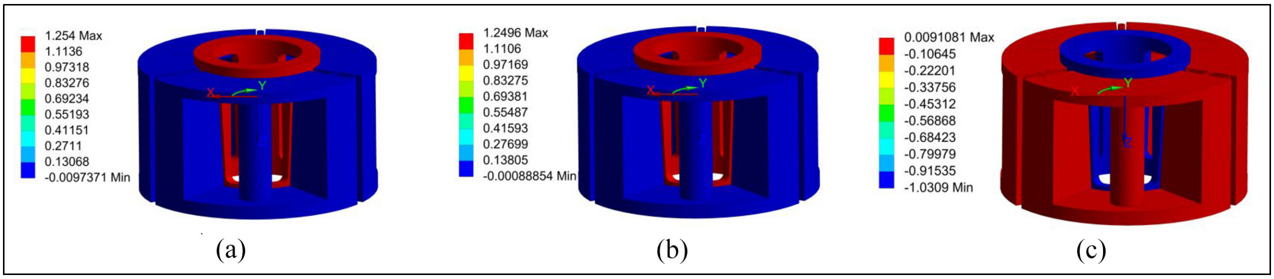

Figure 5. Axial displacement contour of taper sleeve in H3K-40K-104 FEM model /unit: mm: (a) taper sleeve has been inserted (1.254 mm); (b) self-lock status under 400 Nm load (1.2496 mm); (c) non-self-lock status under 400 Nm load (0.0091 mm).

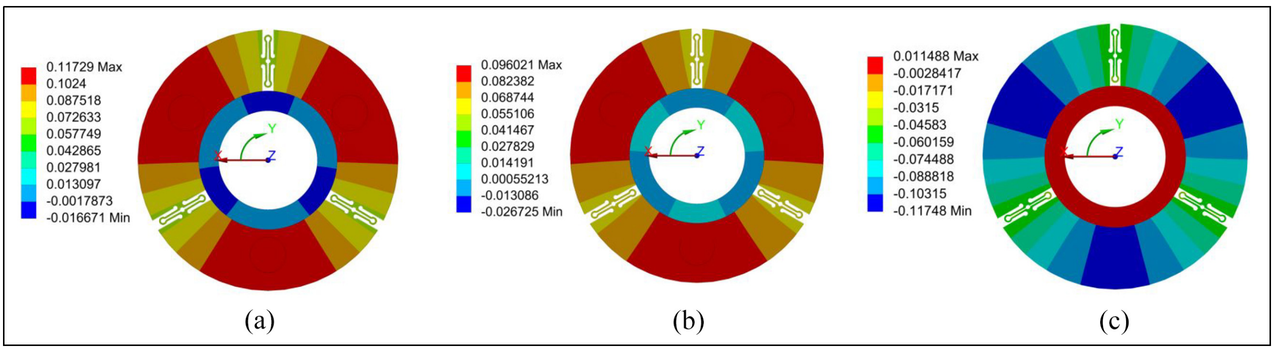

Figure 6. Radial displacement contour of planet shaft in H3K-40K-104 FEM model /unit: mm: (a) taper sleeve has been inserted (0.117 mm); (b) self-lock status under 400 Nm load (0.096 mm); (c) non-self-lock status under 400 Nm load (-0.118 mm).

Figure 7. Contact status contour of output ring gear in H3K-40K-104 FEM model: (a) before taper sleeve insertion; (b) after taper sleeve insertion.

impacts on output accuracy is varying based on their positions within the gear trains. The backlash between the planet gears and ring gears directly affects the output precision of gear trains, whereas that between sun gear and planet gears necessitates consideration of the gear ratio for its influence to be transmitted to the output end. Major variables and definitions used in this section are listed below as Table 4.

For planet- and sun gear pair, the deviation in center distance is denoted as $j_{rsp} = a_{wsp} - a_{0sp}$, where a_{wsp} represents the actual center distance between sun- and planet gear, and a_{0sp} signifies the ideal non-backlash state. The reference center distance a_{sp} between sun- and planet-gear is determined from equation (15). Subsequently, the transverse working pressure angle without backlash α_{0tsp} and with backlash α_{wtsp} are acquired through equation

Table 4. Major variables and definitions list.

Definition	Variables
Transverse modulus	m_t
Transverse pressure angle	α_t
Transverse working pressure angle without backlash	α_{0tsp}
Transverse working pressure angle with backlash	α_{wtsp}
No backlash center distance (Sun- & planet- gear)	a_{0sp}
Reference center distance (Sun- & planet- gear)	a_{sp}
Actual center distance (Sun- & planet- gear)	a_{wsp}
Deviation between actual center distance and no backlash center distance (Sun-, Fix ring-, Output- & planet- gear)	j_{rsp} j_{rfp} j_{rop}
Deviation between actual center distance and no backlash center distance after center distance compensation (Sun-, Fix ring-, Output- & planet- gear)	j'_{rsp} j'_{rfp} j'_{rop}
Circumferential backlash (Sun-, Fix ring-, Output- & planet- gear)	j_{csp} j_{cfp} j_{cop}
Pitch circles radius of sun gear	r'_s
Pitch circles radius of output ring gear	r'_o
Pitch circles radius of fix ring gear	r'_f
Angular backlash between sun gear & planet gear	$\Delta\theta_s$
Angular backlash between output ring gear & planet gear	$\Delta\theta_o$
Angular backlash between fix ring gear & planet gear	$\Delta\theta_f$
Equivalent total output angular backlash at output shaft	Δ
Equivalent sun gear angular backlash at output shaft	Δ_s
Equivalent output ring gear angular backlash at output shaft	Δ_o
Equivalent fix ring gear angular backlash at output shaft	Δ_f

(16). The correlation between circumferential backlash j_{csp} and j_{rsp} is expressed by equation (17).

$$a_{sp} = \frac{1}{2} m_t \left(z_s + z_p\right) \tag{15}$$

$$\begin{cases} \alpha_{0tsp} = \arccos \dfrac{a_{sp} \cdot \cos \alpha_t}{a_{0sp}} \\ \alpha_{wtsp} = \arccos \dfrac{a_{sp} \cdot \cos \alpha_t}{a_{wsp}} \end{cases} \tag{16}$$

$$j_{rsp} = \frac{\cos \alpha_{0tsp} - \cos \alpha_{wtsp}}{2 \cos \alpha_{0tsp} \cdot \left(\mathrm{inv}\alpha_{wtsp} - \mathrm{inv}\alpha_{0tsp}\right)} \cdot j_{csp} \tag{17}$$

Consider the involute function, and the difference between α_{wtsp} and α_{0tsp} is tiny, two approximation equations (18) and (19) are given to simplify equation (19) for convenience in engineering.

$$\begin{cases} \lim\limits_{\alpha_{0tsp} - \alpha_{wtsp} \to 0} \dfrac{\mathrm{inv}\alpha_{wtsp} - \mathrm{inv}\alpha_{0tsp}}{\alpha_{wtsp} - \alpha_{0tsp}} = \sec^2\alpha_{0tsp} - 1 = \tan^2\alpha_{0tsp} & (18) \\ \lim\limits_{\alpha_{0tsp} - \alpha_{wtsp} \to 0} - \dfrac{\cos\alpha_{wtsp} - \mathrm{inv}\alpha_{0tsp}}{\alpha_{wtsp} - \alpha_{0tsp}} = \sin\alpha_{0tsp} & (19) \end{cases}$$

Therefore, the simplified center distance deviation equation between sun- and planet gear, is noted as j_{csp}, can be calculated. Similarly, that of fix ring- and planet gear, and output ring- and planet gear can be conducted following the same way. j_{cop} and j_{cfp} are also given by equation (20).

$$\begin{cases} j_{csp} = 2 j_{rsp} \tan \alpha_{0tsp} \\ j_{cop} = 2 j_{rop} \tan \alpha_{0top} \\ j_{cfp} = 2 j_{rfp} \tan \alpha_{0tfp} \end{cases} \tag{20}$$

Convert the circumferential backlash to angular backlash at sun gear, output ring gear and fix ring gear respectively. $r'_s = \dfrac{z_s}{z_s + z_p} a_{0sp}$, $r'_o = \dfrac{z_o}{z_o - z_p} a_{0op}$ and $r'_f = \dfrac{z_f}{z_f - z_p} a_{0fp}$ are the radius of pitch circles in equation (21).

$$\begin{cases} \Delta\theta_s = \dfrac{j_{csp}}{r'_s} \\ \Delta\theta_o = \dfrac{j_{cop}}{r'_o} \\ \Delta\theta_f = \dfrac{j_{cfp}}{r'_f} \end{cases} \tag{21}$$

Each angular backlash compared with planet gear $\Delta\theta_s$, $\Delta\theta_o$ and $\Delta\theta_f$ can be equivalent to a total output angular backlash Δ by reduction ratio. The relationship is given by equations (22) and (23):

$$\Delta = \Delta_s + \Delta_o + \Delta_f \tag{22}$$

$$\begin{cases} \Delta_s = \Delta\theta_s \cdot \dfrac{z_s\left(z_f - z_o\right)}{z_o\left(z_s + z_f\right)} \\ \Delta_o = \Delta\theta_o \\ \Delta_f = \Delta\theta_f \cdot \dfrac{z_f\left(z_s + z_o\right)}{z_o\left(z_s + z_f\right)} \end{cases} \tag{23}$$

Table 5. H3K-40K-104 prototype anti-backlash effect analysis.

Status No.	Initial				Adopt DPCS			
	j_{rsp} (μm)	j_{rop} (μm)	j_{rfp} (μm)	Equivalent backlash Δ (arcmin)	j'_{rsp} (μm)	j'_{rop} (μm)	j'_{rfp} (μm)	Equivalent backlash Δ (arcmin)
1	10	10	10	1.454	20	0	0	0.073
2	10	9	10	1.506	20	0	1	0.125
3	10	8	10	1.558	20	0	2	0.177
4	10	7	10	1.611	20	0	3	0.229

After backlash compensation, center distance deviation on each gear pair is affected by Δj_r. Backlash compensation model then be described as equation (24).

$$\begin{cases} j'_{rsp} = j_{rsp} + \Delta j_r \\ j'_{rop} = j_{rop} - \Delta j_r \\ j'_{rfp} = j_{rfp} - \Delta j_r \\ \Delta j_r = \min\left(j_{rsp}, j_{rfp}\right) \end{cases} \tag{24}$$

As a result, angular backlash induced by Δj_r on ring gears is much bigger than that of on sun gear. Their ratio is derived as equation (25).

$$\begin{cases} \dfrac{\Delta_o}{\Delta_s} = \dfrac{\sin\alpha_{0top}}{\sin\alpha_{0tsp}} \cdot \dfrac{z_f + z_s}{z_f - z_o} \\ \dfrac{\Delta_f}{\Delta_s} = \dfrac{\sin\alpha_{0tfp}}{\sin\alpha_{0tsp}} \cdot \dfrac{z_o + z_s}{z_f - z_o} \end{cases} \tag{25}$$

In practice, this backlash compensation model is utilized to analyze the backlash of prototype H3K-40K-104. In the gear manufacturing, precise center distance control is crucial to gearbox assembly. A center distance ranges from $5\mu m$ to $15\mu m$ is allowed for ring and sun gears to accommodate machining errors and possible tooth interference in installation process.

Assume an ideal condition is designated as $j_{rop} = j_{rfp} = j_{rsp} = 10\mu m$ in H3K-40K-104 prototype and solve equations (15-25) according to the data provided by Table 2. The given center distance configuration will induce 1.454 arcmin angular backlash at output shaft. However, with the implementation of DPCS, this number dramatically decreases to 0.073 arcmin (4.38 arcsec). This improvement is achieved by carrier extension and planet gear position adjustment, which decreases j'_{rop} and j'_{rfp} to $0\mu m$, and increases j'_{rsp} to $20\mu m$. Equation (25) illustrates that ring gears has more significant influence than sun gear on equivalent backlash, owing to the 3 K gear reduction ratio relationship, as evidenced by the result of $\Delta_o/\Delta_s = 18.7$ and $\Delta_f/\Delta_s = 24.6$. It is apparent that DPCS effectively transfers the center distance deviation to the high-speed shaft where generates the minimal equivalent output backlash. Except compensating for initial deviation, DPCS ensures that gear wear on ring gears is continuously transferred and accumulated onto the sun gear, thereby the impact of tooth profile degradation is greatly relieved.

Additionally, the difference on center distance deviation between two ring gears also induces extra equivalent backlash. Assume a situation that the difference between j_{rfp} and j_{rop} is $3\mu m$, which notes as $j_{rfp} - j_{rop} = 3\mu m$. The equivalent backlash at output end increases from 0.073 arcmin–0.229 arcmin theoretically. Table 5 gives more detailed anti-backlash effect analysis based on the backlash compensation model above, and its related bar charts are shown in Figure 8.

Prototype experiment test

Sample preparation

In order to further prove the feasibilities of DPCS and validate its potential, we developed and produced the first H3K Gear prototype with rated torque 400 Nm and reduction ratio 104, which is encoded as H3K-40K-104. This prototype adopts Wolfrom-based structure, and equips DPCS to restrain backlash on ring gears. Main bearing uses integrated design to make structure compact. No ball bearing is used on sun gear side in this test section.

Three H3K Gear samples (Figure 9) are used in experiments, which share the same lubrication condition. Sample numbers are noted as #1, #2, #3 for convenience. It is worth noting that, to acquire optimal anti-backlash effect, two ring gears are matched and selected according to measured center distance to the same planet gear group. Table 6. gives theoretical backlash values of sample according to backlash compensation model above.

Test equipment and test environment

In this section, the feasibility of H3K Gear and its design will be shown, and comprehensive performance and capacities can be further proved.

The performance test system is presented in Figure 10, the tested H3K Gear is installed between two pairs

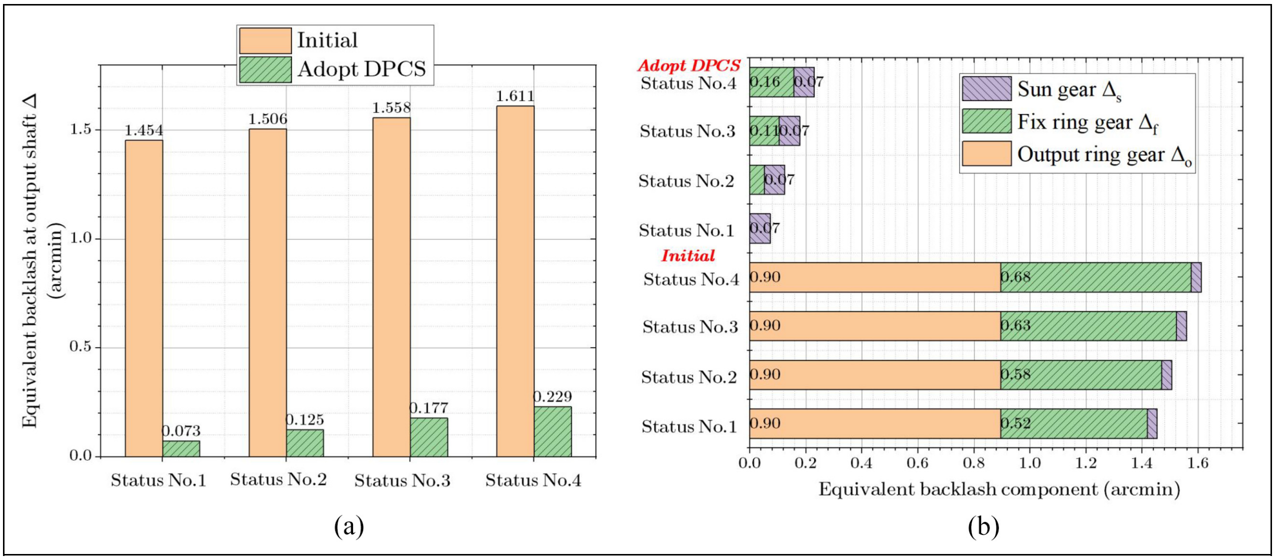

Figure 8. H3K-40K-104 prototype equivalent backlash comparison, (a) Overall equivalent backlash under Status No.1 – No.4 at output shaft; (b) The equivalent backlash of sun gear, fix ring gear and output ring gear under Status No.1 – No.4 at output shaft.

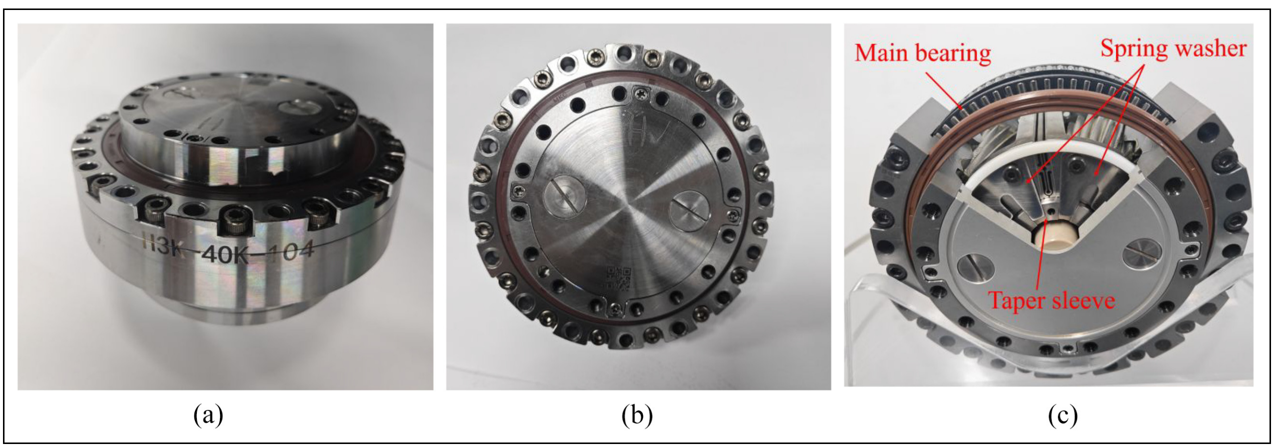

Figure 9. H3K-40K-104 prototype aspects, (a) side; (b) back; (c) section.

Table 6. H3K-40K-104 sample backlash table.

Sample Number	j (μm)	$j_f - j_o$ (μm)	Theoretical backlash (arcsec)
#1	20.4	0.2	5.074
#2	11.5	0.3	3.448
#3	12.6	0.1	3.060

of high-precision angle encoder and torque sensor, which measures real-time angular displacement and torque respectively at both input and output end of H3K Gear. In this experiment test, torsional stiffness, hysteresis characteristic and transmission accuracy can be obtained. Angle encoders are installed closed to tested gearbox in case of displacement measure error caused by torque sensor deformation. An extra precision planetary gearbox installed at output side it to enlarge load torque according to experiment requirement. The test environment for precision is at a room temperature of 24°C and a relative humidity of less than 70%. Further equipment details are given in Table 7.

Test result

Dynamic transmission error measurement

Dynamic transmission error (*DTE*) refers to the angular displacement difference between actual motion and theoretical motion at output end during the stable rotation period of gearbox. In this experiment, real-time rotational angle difference is measured within even input

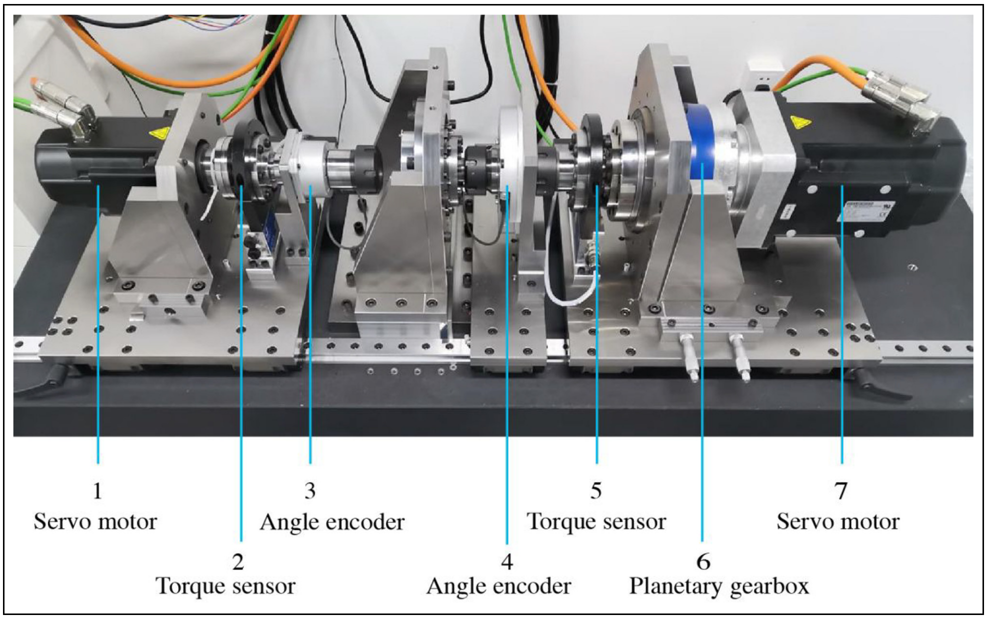

Figure 10. Performance test system.[9]

Table 7. Key equipment and measurement parameters of the performance test system.[9]

Position	Number	Equipment	Manufacturer	Measurement Parameter
Input	1	Servo motor	Kollmorgen, America	2.62 kW, rated torque 10 Nm, peak torque 30 Nm, 27 b resolution, precision 0.33 arcmin
	2	Torque sensor	HBM, German	Accuracy: ±0.03%. Equipped with a dedicated four-channel frequency measurement amplifier, the signal bandwidth is 20 kHz, and the frequency measurement deviation is 0.01%
	3	Angle encoder	HEIDENHAIN, German	28 b absolute value, system accuracy ±2 arcsec
Output	4	Angle encoder	HEIDENHAIN, German	Absolute value type 29 bits, system accuracy ±1 arcsec
	5	Torque sensor	HBM, German	Accuracy: ±0.03%. Equipped with a dedicated four-channel frequency measurement amplifier, the signal bandwidth is 20 kHz, and the frequency measurement deviation is 0.01%
	6	Planetary gearbox	Wittenstein, German	Reduction ratio 50, rated torque 1400 Nm, maximum torque 1760 Nm, hysteresis 1 arcmin
	7	Servo motor	Kollmorgen, America	5.25 kW, rated torque 33.4 Nm, peak torque 110 Nm, 27 b resolution, precision 0.33 arcmin

speed (30)rpm and free load condition. After defining reference angular ordinate and initializing zero-point, servo motor drives gearbox to clockwise rotate (360) degrees on output end, then anticlockwise rotate to its start point. Output encoder notes down actual motion θ_2, and then calculate the difference with that of input encoder θ_1 considering reduction ratio i. Real-time DTE then can be calculated as θ_e by equation (26). The biggest data deviation in curve is defined as Maximum dynamic transmission error (DTE_{max}). Test curves of three samples are illustrated as Figure 11.

$$\theta_e = \theta_2 - \frac{\theta_1}{i} \tag{26}$$

(Figure 11) It is can be seen that H3K-40K-104 prototypes reach low DTE within 25 arcsec and that of traditional planetary gearbox usually ranges from 2 to 4 arcmin.[8] DPCS makes DTE dramatically decrease

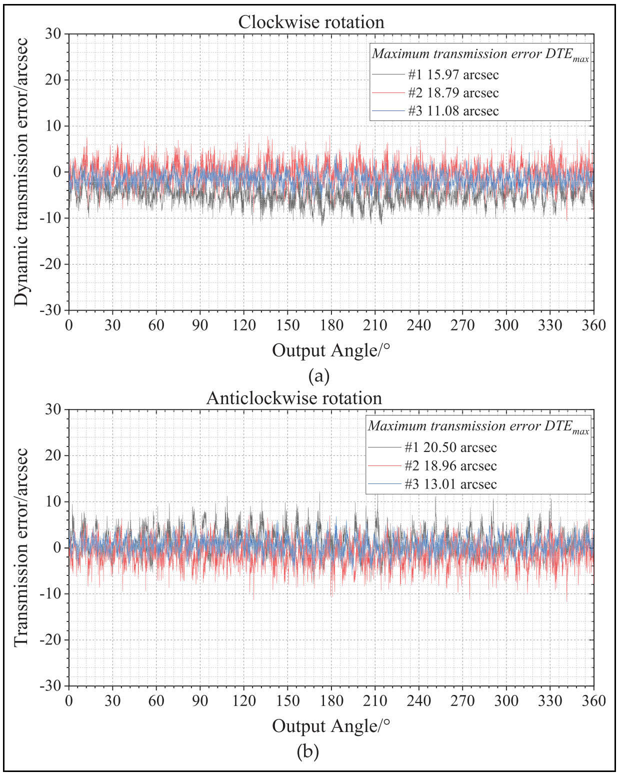

Figure 11. Transmission error curves of three H3K-40K-104 samples #1, #2 and #3respectively, (a) clockwise; (b) anticlockwise.

about 80% compared with traditional design, because anti-backlash condition restrains tooth vibration during engagement period, which ensures smooth torque transmission.

Positioning error measurement

Positioning error (*PE*) represent the accuracy of movement and positioning between multiple targeted points, and it is measured at no-load status. In this experiment, servo motor will drive gearbox to output 380° clockwise and anticlockwise respectively. The commence point and return point are defined as the $-10°$ and 370°. Each unidirectional movement is divided into 37 target positioning points, range from 0° to 360°, with gap 10°, where *PE* data will be recorded. The process of movement between two target point smoothly accelerates or deaccelerates, and maintains a constant maximum input speed 1000 rpm. Similarly, encoder installed at output shaft notes down real output angle at each theoretic target point after gearbox stably stops. Repeat the experiment process three times and the mean values and standard difference of *PE* then can be acquired. During this reciprocating movement, the difference of mean *PE* in clockwise and anticlockwise movement defined as mean backlash. Figure 12 illustrates the *PE* and mean backlash result of three H3K-40K-104 samples.

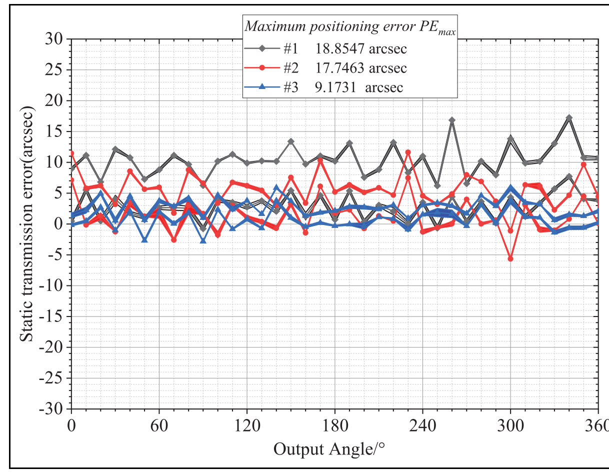

Figure 12. Positioning error curves of three H3K-40K-104 samples #1, #2, and #3 respectively.

Table 8. reveals the backlash of H3K samples is within 6.561 arcsec, which closes to theoretical values, and the maximum positioning error can be controlled within 20 arcsec. When considering the measuring error of HEIDENHAIN angle encoders integrated into the performance test system, it is noted that the errors are ± 2 arcsec at input end and ± 1 arcsec at output end. The measured mean backlash and theoretical backlash conducted by previous model appear strong trend correlation, and their deviation remains within the bounds of the measuring error. Additionally, the installation error of the gearbox, measurement error on tooth parameters are other possible factors that could contribute to the discrepancies.

Stiffness hysteresis test

The stiffness hysteresis characteristic serves as a valuable tool for presenting the static performance of reduction gears in industrial applications. To analyze this characteristic, the input shaft of the tested gearbox is fixed, and a clockwise load torque is gradually applied to the output shaft until reaching the rated torque of 400 Nm. Subsequently, the torque is gradually unloaded to zero and reloaded in the opposite direction to -400 Nm (with the negative symbol denoting the anticlockwise direction). After unloading to zero again, it is reloaded following the same process as the initial loading until the load torque reaches 400 Nm. An encoder installed at the output end records the entire angular displacement, enabling the plotting of a stiffness hysteresis curve. In data analysis process, mean angular displacement between output torque at $\pm$ 3% rated torque on curve is defined as the geometric lost motion

Table 8. Positioning error data analysis.

Sample Code	Maximum positioning error (arcsec)	Mean backlash (arcsec)	Theoretical backlash (arcsec) *quote from Table 4.
#1	18.8547	6.561	5.074
#2	17.7463	3.434	3.448
#3	9.1731	1.657	3.060

Table 9. Stiffness hysteresis test data under rated torque (400 Nm).

Sample Code	K1 stiffness (Nm/arcmin)	K2 stiffness (Nm/arcmin)	K3 Stiffness (Nm/arcmin)	Lost motion (arcsec)	Hysteresis Loss (arcsec)
#1	60.693	90.986	124.78	20.0132	15.6475
#2	66.581	88.132	115.61	17.3216	15.0295
#3	79.622	91.17	117.24	17.2793	11.3337
#1 remove spring washer	39.887	85.851	121.818	76.344	56.696

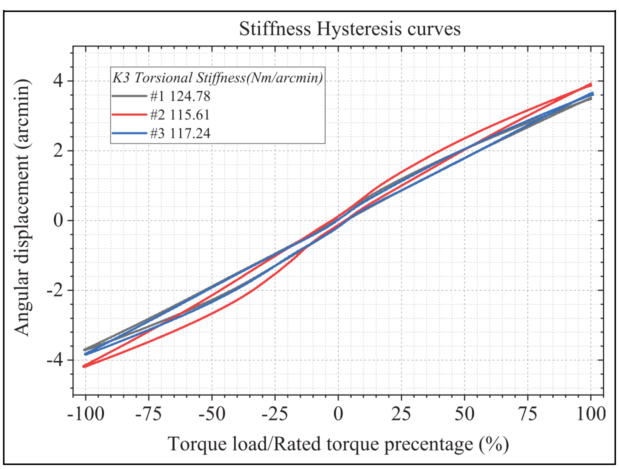

Figure 13. Stiffness Hysteresis curves of three H3K-40K-104 samples #1, #2, and #3 respectively.

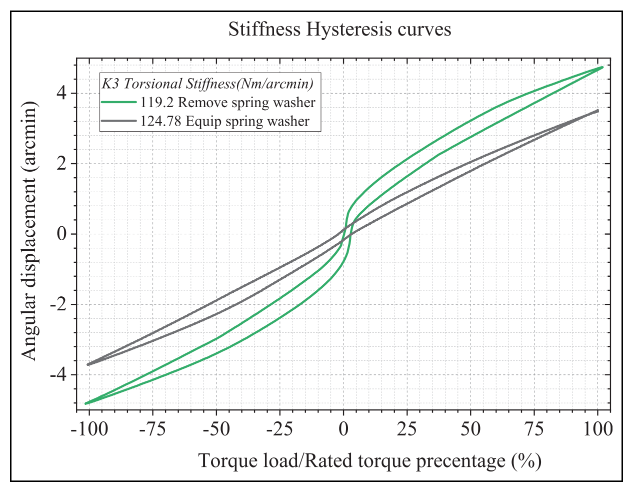

Figure 14. Stiffness hysteresis curves of H3K-40K-104 #1 based on spring washer status.

of tested sample. In addition, angular displacement difference when torque load reach zero is defined as hysteresis loss. The two parameters are affected by many factors, such as backlash, oil film resistance and internal friction, that can be treated as static precision performance of gearbox. The comprehensive torsion stiffness is defined as the ratio of the total torque load to the bandwidth of displacement during the load cycle.

The experiment result (Figure 13) demonstrates that H3K Gear has low-backlash characteristic, as evidenced the curve behavior under low torque loads. The gradient of the curve represents the torsional stiffness at each measure point. Owing to its anti-backlash properties, H3K Gear exhibits a commendable stiffness consistency across various torque conditions. Define K1, K2 and K3 stiffness by the mean value of segmental stiffness on bilateral direction at range 0%–15%, 15%-50% and 50%-100% rated torque respectively.

To reflect the low backlash characteristic in stiffness curve, reinstall the DPCS in sample H3K-40K-104 #1 but remove its spring washer. In this case, carrier is regarded as rigid due to self-lock phenomenon, but it cannot adjust center distance and restrain backlash. By comparison, Figure 14 reveals a significant increase on lost motion (from 20.0132 arcsec to 76.344 arcsec) and hysteresis loss (from 15.6475 arcsec to 56.696 arcsec). The complete stiffness hysteresis test data of four test curves are collected in Table 9 for comparison.

Discussion

In this study, a novel 3 K planetary gearbox anti-backlash mechanism DPCS is proposed. Compared with traditional structure, deformable planetary carrier system enables to adjust gear center distance to effectively compensate backlash caused by wearing, machining error and assembly error. Taper sleeve design, based on self-lock principle, is to prevent carrier shrinkage caused by torque load, maintaining great precision retaining ability under load.

Static model and backlash compensation model give a holistic perspective about structural feasibility and anti-backlash efficacy. Backlash present in the ring gear significantly impacts output precision, whereas that influence in sun gear is minimal and can be neglected due to geometric and kinematic relationships within 3 K gear trains. Center distance compensation decreases 20–30 times comprehensive output backlash, and dramatically increases precision. Finite element method reveals the self-lock characteristic of carrier, which enables to well restrain backlash under load condition.

Prototype experiment results demonstrate a distinct reduction in backlash characteristics, with the dynamic transmission of H3K-40K-104 measuring less than 20.5 arcsec. Additionally, lost motion and mean backlash also perform 20.0132 arcsec and 6.561 arcsec respectively, aligning closely with theoretical value. These finding prove the structure advantages and model feasibility. Therefore, DPCS emerges as an effective method to tackle the precision issue within the 3 K planetary structure, presenting a new R&D direction for the next generation of gearbox. By implementing the Deformable Planet Carrier System, the H3K Gear system showcases a forward-looking approach to addressing precision-related challenges in gear mechanisms. This innovative design not only enhances transmission accuracy and minimizes lost motion but also demonstrates a strategic balance between performance optimization and load-bearing capacity.

To fully leverage the capabilities of H3K Gear, there are some plans of further studies and experiments. Areas that could benefit from further exploration include carrier vibration, backdrivability, impact response, precision over the product's lifetime, load distribution, and noise characteristics. Moreover, investigating the precise correlations among spring parameters, the anti-backlash effect, and the overall gearbox performance stands out as a crucial research avenue for H3K Gear. This research direction aims to delve into a more comprehensive set of advantages on design stage and maximize the potential of the 3 K gear system.

Patents

[1] LING, Zilong. DISPLACEMENT PLANETARY CARRIER SYSTEM AND PLANETARY TRANSMISSION DEVICE THEREOF[P]. Tianjin City CN113757349A, 2021-12-07. (In Chinese)

[2] LING, Zilong. DISPLACEMENT PLANETARY CARRIER SYSTEM AND PLANETARY TRANSMISSION DEVICE THEREOF[P]. WO2023065072,2023-04-27.

Author Contributions

Conceptualization, Z.L.; methodology, Z.L.; software, L.Z. and Y.Z.; validation, D.X. and Y.L.; formal analysis, L.Z. and Y.Z.; investigation, L.Z., D.X. and Y.L.; resources, X.X. and Z.L.; writing—original draft preparation, Y.Z.; writing—review and editing, D.X. and L.Z.; visualization, Z.J., S.X. and Y.Z.; supervision, Z.L. and D.X.; project administration, Z.L. and Y.L.; funding acquisition, Z.L.; All authors have read and agreed to the published version of the manuscript.

Declaration of conflicting interests

The author(s) declared no potential conflicts of interest with respect to the research, authorship, and/or publication of this article.

Funding

The author(s) received no financial support for the research, authorship, and/or publication of this article.

ORCID iD

Yi Zhou https://orcid.org/0009-0005-0563-3178

Data Availability Statement

The data that support the findings of this study are available from the corresponding author upon reasonable request.

References

1. García PL, Crispel S, Saerens E, et al. Compact gearboxes for modern robotics: a review. *Front Rob AI* 2020; 7: 103.
2. Alessandro De L. U. C. A. and Book W. A. Y. N. E. J. *Robots with flexible elements*. Heidelberg: Springer Handbook of Robotics, 2008. 243–282.
3. Asadi E, Li B and Chen I-M. Pictobot: a cooperative painting robot for interior finishing of industrial developments. *IEEE Robot Autom Mag* 2018; 25: 82–94.

4. Ill-Woo P, Jung-Yup K, Jungho L, et al. "Mechanical design of humanoid robot platform KHR-3 (KAIST Humanoid Robot 3: HUBO),"*Proc. 5th IEEE-RAS Int. Conference on Humanoid Robots*, pp. 321-326, 2005.
5. Wensing PM, Wang A, Seok S, et al. "Proprioceptive actuator design in the MIT cheetah: impact mitigation and High-bandwidth physical interaction for dynamic legged robots,"
6. Butunoi PA, Stan G, Ciofu C, et al. Research regarding backlash improvement for planetary speed reducers used in the actuation of industrial robots. *Appl Mech Mater* 2016; 834: 114–119.
7. Mousavi A, Akbarzadeh A, Shariatee M, et al. Repeatability analysis of a SCARA robot with planetary gearbox. In: *RSI International Conference on Robotics and Mechatronics ICRoM*, 2015, pp. 640–644 .
8. Litvin FL and Feng PH. Computerized design and generation of cycloidal gearings. *Mech Mach Theory* 1996; 31: 891–911.
9. Sensinger JW and Lipsey JH. Cycloid vs. harmonic drives for use in high ratio, single stage robotic transmissions. In *Proc. IEEE Int. Conf. Robot. Automat.*, 2012, pp. 4130–4135.
10. Shuai M, Shuai M, Guoguang J, et al. Design principle and modeling method of asymmetric involute internal helical gears. *Proc IMechE, Part C: J Mechanical Engineering Science* 2019; 233: 244–255.
11. Velex P and Ville F. An analytical approach to tooth friction losses in spur and helical Gears—influence of profile modifications. *J Mech Des* 2009; 131: 101008–101009.
12. Litvin FL, Vecchiato D, Demenego A, et al. Design of one stage planetary gear train with improved conditions of load distribution and reduced transmission errors. *J Mech Des* 2002; 124: 745–752.
13. Litvin FL and Hsiao CL. Computerized simulation of meshing and contact of enveloping gear tooth surfaces. *J Appl Mech Eng* 1993; 102: 337–366.
14. Getachew A. The performance of gear with backlash: a review. *J Appl Mech Eng* 2021; 10: 389.
15. Prajapat GP, Senroy N and Kar IN. Modeling and impact of gear train backlash on performance of DFIG wind turbine system. *Elect Power Syst Res* 2018; 163: 356–364.
16. Feng K, Ji JC, Ni Q, et al. A review of vibration-based gear wear monitoring and prediction techniques. *Mech Syst Signal Process* 2023; 182: 10–15.
17. Sreepradha C, Krishna Kumari A, Elaya Perumal A, et al. Neural network model for condition monitoring of wear and film thickness in a gearbox. *Neural Comput Appl* 2014; 24: 1943–1952.
18. Feng K, Ji JC, Zhang Y, et al. Digital twin-driven intelligent assessment of gear surface degradation. *Mech Syst Signal Process* 2023; 186: 16–20.
19. Nordin M and Gutman PO. Controlling mechanical systems with backlash—a survey. *Automatica* 2002; 38: 1633–1649.
20. Ai X. "Planetary traction drive transmission," U.S. Patent 6,406399 B1, jun. 18, 2002.
21. Oba S and Fujimoto Y. Hybrid 3K compound planetary reduction gearbox with a roller transmission mechanism. *IEEE/ASME Trans Mechatron* 2022; 27: 2356–2366.
22. Ling Z, Zhao L, Xiao D, et al. A Novel strain wave gear reducer with double flexsplines. *Actuators* 2023; 12: 313.
23. Wang G, Zhu D, Zou S, et al. Simulation and experimental research on electrical control anti-backlash based on a novel type of variable tooth thickness involute gear pair. *Stroj. vestn.-J. Mech. Eng* 2022; 68: 126–140.
24. Penčić M, Čavić M and Borovac B. Development of the low backlash planetary gearbox for humanoid robots. *FME Trans* 2017; 45: 122–129.
25. Georgiev NZ. Towards high performance robotic actuation (Ph.D. thesis), *Caltech*, 2019.
26. Wolfrom U. Der Wirkungsgrad von Planetenradergetrieben. *Werkstattstechnik*, Vol.V1, 1912